ELSEVIER

International Journal of Mass Spectrometry 185/186/187 (1999) 883–903

International Journal of Mass Spectrometry

Molecular dynamics simulation of gas phase ion cluster formation

Orlando M. Cabarcos, James M. Lisy*

Department of Chemistry, University of Illinois at Urbana-Champaign, Urbana, IL 61801, USA

Received 4 August 1998; accepted 12 October 1998

Abstract

The structure, energetics, and dynamics of gas phase cluster ions formed by the collision between an atomic ion, Cs^+, and a neutral molecular cluster, have been characterized using molecular dynamics simulations. These studies have shown that cluster ions stabilize by evaporative cooling, i.e. the loss of a molecule, to dissipate excess internal energy within the nascent cluster ion. Particular emphasis has been placed on characterizing the distribution of internal energy within the cluster ion and how subsequent evaporative steps affect that distribution. The mechanism of the evaporative process and the time scale associated with the formation of the first solvent shell around the ion were also investigated. (Int J Mass Spectrom 185/186/187 (1999) 883–903) © 1999 Elsevier Science B.V.

Keywords: Metal ion solvation; Solvating collisions; Cluster ions; Solvation dynamics; $Cs^+(CH_3OH)_n$

1. Introduction

The formation process of gas-phase cluster ions is of fundamental interest because of the unusual properties associated with these species. The strong noncovalent ion-neutral interaction can lead to substantial binding energies on the order of 0.5 eV. Additionally, the intrinsic charge on the cluster ion allows almost total experimental control over the system using mass spectrometric methods. As a result, cluster ions can be studied over time scales that span 12 orders of magnitude, from elegant picosecond pump–probe experiments as exemplified by Syage and co-workers [1], to the fascinating ion-trap studies of Dunbar [2–4], McMahon [4,5], and Bondybey [6,7], where ion clusters undergo unimolecular dissociation over periods of seconds after absorbing blackbody radiation. This combination of considerable internal energy content with almost arbitrary observational time scales has focused attention on methods of energy dissipation in these finite-sized systems. On the nano to microsecond time scale, the predominant mechanism is evaporative loss of a neutral component of the cluster ion, although intracluster chemical reactions are also possible [8–12].

A common theme in the determination of internal energy distributions in these systems involves the use of the evaporative ensemble, first popularized by Klots [13–15]. Many groups have applied this concept to a wide variety of cluster ions. Recent examples

* Corresponding author. E-mail: j-lisy@uiuc.edu

Dedicated to Professor Michael T. Bowers on the occasion of his 60th birthday.

PII S1387-3806(98)14212-4

from the literature have involved pure systems such as Li_n^+ and Te_m^+ by Bréchignac and co-workers [16,17], and solvated systems such as $Mg^+(H_2O)_n$ by Fuke et al. [11,12,18]. Investigations in our laboratory have previously focused on structural properties of simple ions: Na^+ and Cs^+, solvated by CH_3OH or NH_3, by means of infrared laser spectroscopy and Monte Carlo simulations [19–23].

In an attempt to bridge the experimental studies on cluster ions in our group and others with the statistical treatments of cluster evaporation, we have applied molecular dynamics methods to cluster ion formation [24]. In addition, the simulations lead to an insightful and more molecular-based perspective of the cluster ion formation process. Particularly relevant to this current effort are early studies on proton hydration dynamics of $(H_2O)_8$ by Stillinger and Weber [25,26], and the work by Stace and Del Mistro on the collision between acetonitrile and a cluster of argon atoms [27]. The extent of fragmentation, final cluster composition, and evaporative cooling are among some of the issues addressed in these earlier articles. In our previous investigation [24], we observed that two types of collisional processes were possible: a ballistic collision that involves a shattering of the neutral cluster upon impact with the ion; and a viscid or sticky collision where the ion is enveloped by the neutral cluster, with subsequent evaporative loss. In a recent study of collision dynamics between water clusters [28], similar behavior was observed for small impact parameters.

In this study, we have expanded upon these earlier efforts in a number of directions. First, we extended the structural analysis to include the orientational configuration of the solvent that is relevant to shell formation. Second, a systematic study of structure and energetics was conducted to examine the role of evaporative cooling for a specific set of cluster ions through two successive evaporative losses. Finally, the criteria for an evaporative loss were refined from our earlier approach to more precisely define the point in time of evaporation. This had only a minor effect (1–3%) on previously determined properties, such as the final cluster distribution, and left our conclusions from the earlier study unchanged [24].

2. Simulation methods

Simulations were performed on the collision between a Cs^+ ion and a neutral cluster of 20 methanols at eight different center of mass (COM) collision energies: 1, 2, 3, 5.5, 8, 12, 16, and 25 eV. All collisions were conducted at zero impact parameter to better observe the effects attributed solely to variation in collision energy. For similar reasons only a target cluster of twenty methanol molecules was simulated. Varying either of these parameters should have a considerable effect on the cluster ion formation process and the resulting distributions of cluster ion properties. Future work detailing these effects is currently planned.

The MD calculations were done using CHARMM [29] version 24 with customized potential parameters. Five hundred simulations were performed at each collision energy with each set of 500 broken down into 10 sets of 50 simulations. Each of the 10 sets used a different initial starting configuration for the $(CH_3OH)_{20}$ cluster. Although the same initial structure was used over each of 50 runs, a statistical distribution was assured by randomly placing the ion on the surface of a large sphere centered at the COM of the methanol cluster. The individual simulations were run for 100 ps. The results of the 500 runs were then averaged together, by final ion cluster size, to give a statistical distribution of ion cluster energies and cluster fragmentation patterns. The average properties over the 500 simulations were then compared and contrasted based on collision energy.

Each individual simulation was also apportioned into different stages, with each stage defined by the occurrence of an evaporative event, as will be described below. This yielded a final cluster ion, a parent cluster ion, and a grandparent cluster ion stage, over which cluster ion properties were calculated. Thus, the system properties could be followed as the cluster ions evolved via evaporation.

Finally, in order to quantify the time scale of the solvation process, radial distribution functions (RDFs) were computed as a function of time. Each simulation was partitioned into picosecond time slices over which the RDFs were computed. The resulting

RDFs were then averaged over all the simulation runs at the same collision energy, to yield an average RDF for each final ion cluster size. A second measure of the solvation time scale was made by following the orientation of the dipole moment vector of each methanol with respect to the radial vector connecting the ion and the methanol COM over time.

2.1. The potential force field

The MD simulations employ a standard pairwise additive Lennard-Jones potential with a coulombic term. Although a polarizable potential is physically more accurate, at present it is too computationally expensive to implement for the large number of simulations required for this study. Nevertheless, the widely used additive Lennard-Jones potential form should provide a semiquantitative picture of the cluster ion formation process. Indeed, a well chosen additive potential force field can accurately predict system properties as well as a more sophisticated polarizable model [30].

The explicit form of the potential energy is,

$$V_{\text{total}} = \sum_{i=1}^{n'} \sum_{j=i+1}^{n'} V(r_{ij})$$

$$= \sum_{i=1}^{n'} \sum_{j=i+1}^{n'} \left[4\epsilon_{ij}\left(\frac{\sigma_{ij}^{12}}{r_{ij}^{12}} - \frac{\sigma_{ij}^{6}}{r_{ij}^{6}} \right) + \frac{q_i q_j}{r_{ij}} \right] \quad (1)$$

where n' is the total number of atoms, r_{ij} is the distance between atom i and atom j, and q_i and q_j are the respective partial charges. The Lennard-Jones parameters, ϵ_{ij} and σ_{ij}, are combined by taking the geometric average of the individual atom parameters,

$$\epsilon_{ij} = (\epsilon_{ii}\epsilon_{jj})^{1/2};\ \sigma_{ij} = (\sigma_{ii}\sigma_{jj})^{1/2} \quad (2)$$

CHARMM also employs two additional energy terms in the potential function of the molecular dynamics (MD) simulation to incorporate flexible molecules. The first involves a harmonic approximation to the bond energy,

$$V_b = \sum k_b(r - r_{\text{eq}})^2 \quad (3)$$

where r_{eq} is the equilibrium bond length and k_b is the bond force constant. The second term applies to the angle energy,

$$V_\theta = \sum k_\theta(\theta - \theta_{\text{eq}})^2 \quad (4)$$

where θ_{eq} is the equilibrium bond angle and k_θ is the angle force constant [29].

The parameters and partial charges used for methanol are the optimized parameters for liquid simulations (OPLS) taken from Jorgensen et al. [31]. The methanol is represented by a three-site model consisting of a polar hydrogen, an oxygen, and a united atom representing the methyl group. The parameters were derived by fitting to experimental data for the pure liquid solvents and give the correct thermodynamic properties and structure. These same parameters also yield reasonably good interaction energies and structures for the gas phase complexes [31]. For the Cs^+ ion parameters, an attempt was made at using a set of parameters developed by Aqvist [32]. This gave results inconsistent with our experimental and Monte Carlo (MC) results from an earlier study of $Cs^+(CH_3OH)_n$ that employed a modified Rittner potential [22]. Using a constant geometry and solvent partial charges, new ϵ and σ parameters for Cs^+ were obtained by fitting the 6–12 potential to the modified Rittner potential. Standard pairwise additive Lennard-Jones and coulombic terms were used to describe the interaction potentials. The parameters for the Cs^+ and the three-site methanol interactions have been used previously in a MC study of $Cs^+((CH_3)_2CO)_n(CH_3OH)_m$ [23]. This parameter set does not explicitly include ion-induced dipole or other nonadditive terms. All the parameters used are listed in Tables 1 and 2.

2.2. Molecular dynamics simulations and analysis

Monte Carlo annealing simulations (using the same additive potential of the MD simulations) were performed to obtain the 10 different configurations of $(CH_3OH)_{20}$ that served as the initial configurations in the MD simulations. Each neutral cluster was mini-

Table 1
Additive potential parameters used in the molecular dynamics simulations

Atom	q (e)	ϵ (kJ mol^{-1})	σ (Å)
		Ion[a]	
Cs^+	1.000	25.3447	2.760
		Methanol[b]	
Me	0.265	0.8661	3.775
O	−0.700	0.7113	3.070
H	0.435	0.0	0.0

[a] [31].
[b] [23].

mized in energy using the adopted basis Newton–Raphson minimization method [29] that was followed by a 10 ps heating period to raise the cluster temperature to 25 K. The neutral cluster was next equilibrated over a 50 ps time scale, prior to serving as the starting point for all collision simulations.

Assigning the appropriate initial velocity to the Cs^+ ion determines the COM collision energy. The ion was then randomly placed on a sphere centered at the COM of the neutral cluster. The radius of the sphere was varied at each collision energy to yield an impact time of 5 ps with the cluster COM. The ion is placed along the x axis of the neutral cluster coordinate frame and is rotated by the three Euler angles, ϕ, χ, and θ, to its random position. All collision simulations were conducted at zero impact parameter. Table 3 lists the initial assigned ion velocities and sphere radii for all eight COM collision energies.

The classical equations of motion were integrated for 100 ps using the Verlet algorithm [33,34]. All bonds containing a hydrogen atom were constrained by the SHAKE algorithm [35] that allowed the use of a 1 fs time step. The nonbonded interactions were cut off at 25 Å using smoothing algorithms to avoid a discontinuity in the energy function. The Lennard-Jones interactions were smoothed using a switching function whereas a shifting function was used for the electrostatic interactions. The simulations were conducted in a reference frame moving at a typical molecular beam velocity of 550 m/s along the impact axis to simulate a neutral methanol cluster prepared in a molecular beam with argon as the carrier gas. In this reference frame, the neutral cluster is stationary. The center of mass (COM) collision energies and the equivalent laboratory frame Cs^+ translational energies are listed in the last row of Table 3.

Table 2
Methanol geometry and harmonic force constants used in the molecular dynamics simulations

Structural parameter[a]	Force constant[b] (kJ mol^{-1} Å^{-2})
R_{MeO} = 1.43 Å	k_b = 1422.6
R_{OH} = 0.945 Å	k_b = 2112.9
∠MeOH = 108.5°	k_θ = 205.0

[a] [31].
[b] These are the default values from CHARMM.

After the completion of all 4000 simulations, each set of 500 runs was analyzed based on the final cluster ion size. The final cluster size was determined by examining the final time step of the simulation. If a molecule was within 51 Å of the ion, it was considered part of the ion cluster. This distance, slightly more than twice the potential cutoff, was chosen to ensure that the methanol molecules are well outside the range of ion influence. Any methanols outside the cutoff were considered dissociated fragments. Similarly, a distance cutoff of 51 Å was used to determine which of these dissociated fragment molecules were in the form of dimers or larger clusters. In this manner, the final cluster ion and neutral fragment distributions were determined. The results for each cluster ion size were averaged after all 500 runs had been processed.

Once the final size of the cluster ion has been determined, the simulation is followed backwards in time to determine at what point each of the dissociated fragments left the ion cluster. These are labeled "evaporative" events, although no evaporation need have occurred, i.e. the fragment may have dissociated upon the initial collision of the ion. (This is especially relevant at the higher collision energies where most of the solvent molecules are lost upon collision.) Each evaporative event is defined by the last negative minimum in COM radial velocity of the fragment with respect to the ion cluster [36] that supplies a time marker. The fragment COM is used because the fragment may consist of a monomer, dimer, or larger size cluster. Additionally, the fragment must be within

Table 3
Initial ion velocities and radii of the spheres used at the various COM collision energies, with the corresponding lab frame translational energy

	COM collision energy (eV)							
	1	2	3	5.5	8	12	16	25
Ion velocity (Å/ps)	13.2	18.7	22.9	31.0	37.4	45.9	53.0	66.2
Sphere radius (Å)	66.2	93.6	114.6	155.2	187.2	229.3	264.8	330.9
Lab frame Cs^+ energy (eV)	2.4	4.0	5.6	9.2	12.7	18.2	23.5	35.4

51 Å of the ion cluster. This accounts for problems attributed to dimer or larger neutral clusters fragmenting after they have evaporated from the cluster. While these criteria were used in the earlier MD report [24], after further analysis they were found to be insufficient. They did not account for neutral fragments that would orbit the cluster ion before being nudged away by an unfavorable interaction. Using the previous criteria as a starting point, the fragment was followed forward in time until it was a minimum of 51 Å away from all the methanols that remain solvating the ion. This was used to mark the evaporative event and define the time of evaporation.

With each fragmentation labeled with an evaporation time, the simulations can be used to determine when the final ion cluster was born. The time window, or equivalently the sample time, for the existence of the final ion cluster is thereby defined as the time between the last evaporative event and the end of the simulation. Similarly, the parent ion cluster survival time is defined as the time between the penultimate evaporative event and the final evaporative event. Finally, the grandparent cluster ion survival time is likewise determined by the third-to-last and penultimate evaporative event. It should be emphasized that it is only possible to measure a sample time for the final ion cluster as opposed to the survival times measured for the parent and grandparent clusters. This is because of the somewhat random nature of the sample time, which is arbitrarily determined by the completion of the simulation. In order to obtain an average parent ion lifetime, the decay of the parent cluster ion population as a function of survival time was fit to a first order exponential decay.

At this point, the final cluster ion size for the simulation has been determined and each evaporative event has been identified. Before the given simulation is analyzed in further detail, it must meet a few additional requirements. In order to average over a significant number of configurations, the final and parent cluster ions must exist for at least 1 ps, otherwise the simulation data for the given run are not processed. (This is not enforced for some of the low energy collisions where no evaporation occurs, i.e. the final cluster ion size is 20.) If the grandparent exists for less than 1 ps, the simulation is still analyzed but the calculations for the grandparent ensemble are not performed. Any simulation is also discarded in which the cluster ion loses a fragment larger than a monomer for the last and penultimate evaporative events. Similarly, if two monomers are lost simultaneously for either of the last two evaporative events, the simulation is skipped. These last two requirements are enforced so that the cluster ion properties can be averaged over similarly evolving cluster ion ensembles. The additional requirements result in fewer than 5% of the simulations being discarded. Finally, if the ion is not solvated there is no final cluster ion to examine, and thus the simulation is skipped. Simulation runs meeting all of the above criteria will have well defined final and penultimate evaporative events with each event consisting of the loss of a single methanol molecule.

In addition to the previously determined final cluster ion size and fragment distributions, the fully qualified simulations are analyzed to ascertain the average total potential energy, the total kinetic energy, and the angular momentum of the cluster ions. The total kinetic energy is also partitioned into its translational, vibrational, and rotational kinetic energy

components. Similar properties are calculated for the methanol monomer fragments that evaporate to form the parent and final cluster ions. Other properties, such as the number of solvents in the first solvation shell, the lab frame translational energy, and the percentage of the total system kinetic energy present in the cluster ion are computed as well.

The total potential energy of the system is determined from Eqs. (1), (3), and (4) above, whereas the total kinetic energy of the cluster ion is calculated using

$$\mathrm{TKE} = \frac{1}{2}\sum_{i}^{n'} m_i v_i^2 \tag{5}$$

where the sum is over the n' atoms present in the cluster ion. The COM position, $\mathbf{R}^c_{\mathrm{COM}}$, and velocity, $\mathbf{V}^c_{\mathrm{COM}}$, of the cluster ion are computed using

$$\mathbf{R}^c_{\mathrm{COM}} = \frac{1}{M^c}\sum_{i}^{n'} m_i \mathbf{r}_i \tag{6}$$

and

$$\mathbf{V}^c_{\mathrm{COM}} = \frac{1}{M^c}\sum_{i}^{n'} m_i \mathbf{v}_i \tag{7}$$

where M^c refers to the mass of the cluster ion and m_i, $\mathbf{r}_i$, and $\mathbf{v}_i$ are the mass, position, and velocity of atom i.

The cluster COM velocity determines the translational energy of the cluster ion. The translational energy contribution to the cluster ion's total kinetic energy can thus be calculated by inserting the cluster mass and cluster COM velocity in an equation analogous to Eq. (5). The remainder of the kinetic energy present in the cluster ion is therefore attributed to the vibrational and rotational kinetic energy components. The rotational energy of the cluster is computed using,

$$\mathrm{KE}_{\mathrm{rot}} = \tfrac{1}{2}\mathbf{J}^t\,\tilde{\mathbf{I}}^{-1}\mathbf{J} \tag{8}$$

where $\mathbf{J}$ is the angular momentum of the cluster,

$$\mathbf{J} = \sum_{i}^{n'} \mathbf{r}_i \times \mathbf{p}_i \tag{9}$$

and $\tilde{\mathbf{I}}$ is the inertia tensor. The moments of inertia are given by

$$I_{jj} = \sum_{i}^{n'} m_i(r_i^2 - r_{ij}^2) \tag{10}$$

and the products of inertia are similarly

$$I_{jk} = I_{kj} = -\sum_{i}^{n'} m_i r_{ij} r_{ik} \tag{11}$$

where j and k represent the x, y, and z axes. The kinetic energy unaccounted for by the cluster translational and rotational kinetic energy must be attributed to the vibrational kinetic energy, $\mathrm{KE}_{\mathrm{vib}}$,

$$\mathrm{KE}_{\mathrm{vib}} = \mathrm{TKE} - \mathrm{KE}_{\mathrm{trans}} - \mathrm{KE}_{\mathrm{rot}} \tag{12}$$

Assuming that the rotational energy is partitioned evenly over the three rotational degrees of freedom of the cluster ion, a rotational temperature can be calculated,

$$T_{\mathrm{rot}} = \frac{2\langle \mathrm{KE}_{\mathrm{rot}}\rangle}{3k_b} \tag{13}$$

where k_b, is the Boltzmann constant. Likewise, a vibrational temperature can be approximated by assuming that $\mathrm{KE}_{\mathrm{vib}}$ is evenly distributed over all the available vibrational modes,

$$T_{\mathrm{vib}} = \frac{2\langle \mathrm{KE}_{\mathrm{vib}}\rangle}{(8N-3)k_b} \tag{14}$$

The number of available vibrational modes in the cluster ion is calculated using $8N - 3$, where N is the number of methanol molecules solvating the ion. Each solvent contributes 8 degrees of freedom to the cluster ion, three per atom (recall that the methyl group is represented by a united atom) minus the SHAKE constrained O–H mode. The ion contributes three additional modes, giving a total of $8N + 3$ modes. Subtracting the translational and rotational modes yields the final expression, $8N - 3$. The term

"temperature" is used as a convenient way to express the average vibrational energy per degree of freedom. By using a three-atom model for methanol and a classical treatment for the resulting vibrational degrees of freedom, such an expression is clearly approximate. However, it is useful in relating the evaporative cooling process and the equilibration of the rotational and vibrational degrees of freedom.

All of the properties described above, in addition to a few others, are calculated and averaged for the final, parent, and grandparent cluster ions for each time step they are in existence. The same properties are computed for the evaporated fragment clusters. The resultant averages are then binned by the final cluster ion size. After all the simulations have been analyzed, the results are averaged over all 500 runs.

In summary, each simulation is cataloged by the COM collision energy at which it was run. The simulations are further cataloged by the resulting final ion cluster size. Numerous properties of the final, parent, and grandparent cluster ions are calculated for each simulation and averaged together with the results from similar runs, i.e. runs at the same collision energy and same final cluster ion size. Similarly, properties of the fragment monomers responsible for the last and penultimate evaporative events are also calculated and averaged.

Two types of structural calculations are also performed. A time-dependent radial distribution function, RDF(t), represents the probability that an oxygen atom on each methanol will be found in a spherical shell of thickness dr at a distance r away from the cesium with respect to a homogenous solution of unit density. The RDF is given by

$$G(r) = \frac{n(r, s)}{V \cdot s \cdot \rho} \tag{15}$$

where $n(r, s)$ are the number of atoms observed in the shell, V is the volume of the shell, s is the total number of time steps in the simulation and ρ is set to 1, corresponding to a solution of unit density. In order to gauge how quickly the solvent shell structure forms around the ion, the RDFs are calculated as a function of time. The first 20 ps of each simulation are divided into 1 ps time slices and an RDF is calculated for each slice. The resulting 20 RDFs are then averaged over all 500 simulations, with respect to the final cluster ion size, to give an averaged RDF(t). These $\langle \text{RDFs}(t) \rangle$ are then integrated to determine solvent shell occupancy numbers.

A second structural measure of solvation time scale can be made by following the orientation of the methanol dipole moment vector with respect to the radial vector connecting the ion and the methanol COM over time [37],

$$\langle \hat{\mu} \cdot \hat{r} \rangle(t) = \langle \cos \theta \rangle(t) \tag{16}$$

The dot product is averaged at each time step over all the solvents. If the dipoles orient towards the ion, the average will approach one. If the ion has no influence on the solvents, the random distribution of the solvents will yield an average approaching zero.

Table 4
Final ion cluster and fragment distribution

Collision energy (eV)	$Cs^+(CH_3OH)_n$ (average n)	Methanol fragment (average size)
1.0	18.6 ± 0.8	1.0 ± 0.1
2.0	16.9 ± 0.9	1.0 ± 0.2
3.0	14.8 ± 1.1	1.1 ± 0.3
5.5	10.3 ± 1.5	1.1 ± 0.4
8.0	7.4 ± 1.7	1.1 ± 0.4
12.0	4.7 ± 1.6	1.1 ± 0.5
16.0	3.0 ± 1.3	1.1 ± 0.4
25.0	1.1 ± 1.0	1.1 ± 0.4

3. Discussion and results

3.1. Cluster ion and fragment size distributions

The cluster ion product distribution was determined by examining the final configuration of the system at the last time step of each simulation. The results presented in Table 4 and Fig. 1 are the simulation equivalent of observing the cluster ion distribution in an experiment, i.e. the product ions are observed at a fixed point in time after the formation (collision) process has occurred. Not surprisingly, the

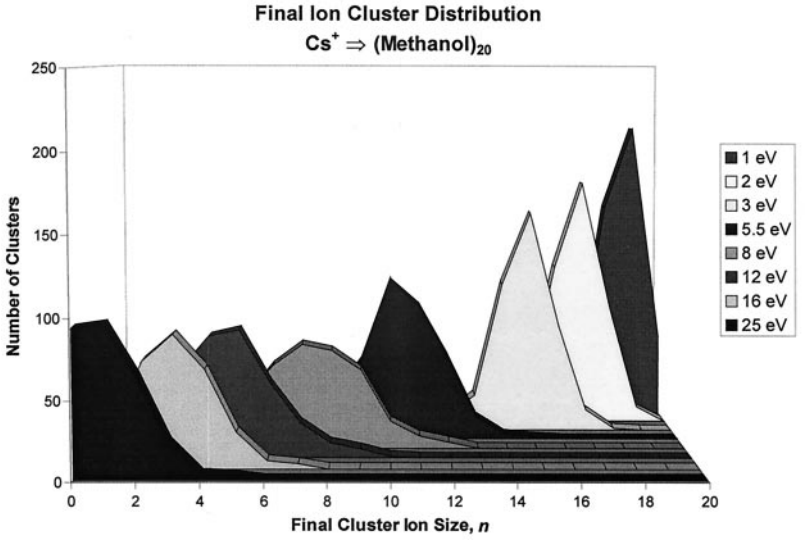

Fig. 1. Histograms of the final ion cluster distribution at eight different collision energies over a 100 ps time scale. The limits are imposed by the finite size of the system.

size distribution of the final ion cluster has a significant dependence on the initial collision energy. The lower energy collisions generate larger ion clusters, whereas the higher energy collisions lead to more fragmentation and smaller ion clusters. The widest observed distribution of cluster ion sizes occurs at a COM collision energy of 8 eV. The revised evaporation criteria did not significantly alter these results from our previous observations [24].

The COM collision energy also determines the distribution of the neutral fragments. Fig. 2(a) displays the percent probability that a methanol molecule will be part of a monomer, dimer, trimer, or tetramer fragment. The lower collision energies yield a preponderance ($>$ 90%) of monomer fragments. Higher energies, in contrast, generate larger neutral fragments, although the majority ($>$ 80%) of the fragments are still monomers. Interestingly, dimer formation maximizes at a collision energy of 8 eV. The presence of a maximum is indicative of two competing processes: (1) As the collision energy increases, more methanols will be lost upon impact and subsequent evaporative cooling events [13–15], leading to the possibility of large neutral fragments, and (2) the energy increase also leads to more energetic neutral fragments that can dissociate to smaller size fragments on the 100 ps time scale of the simulation. These two competing processes also correlate with a minimum in the generation of monomer fragments at 8 eV. Overall, most of the methanols are lost as monomers, either because of the initial impact or evaporative cooling of the cluster ion. Further examination of the simulation data reveals another interesting point; evaporative cooling of the cluster ions proceeds almost exclusively via the loss of methanol monomers. Rarely are dimers or larger fragments lost because of evaporation. Most of the observed dimers, trimers, and larger neutral fragments are formed by the initial ion impact with the $(CH_3OH)_{20}$ cluster and its subsequent fragmentation. This is consistent with experimental observations [38]. Fig. 2(b) displays the accumulated percentage of monomer loss at 5, 15, and 25 ps after the initial collision. In the collisions occurring at 12 eV or above, the cluster ions lose $\sim$ 50% of the monomer fragments within 5 ps of ion impact. By comparison, at collision energies of 5.5 eV or below, the cluster ions lose $\sim$ 20% of their monomers within the same time frame. This indicates that most of the monomer solvent loss in the high energy collisions occurs upon the initial impact,

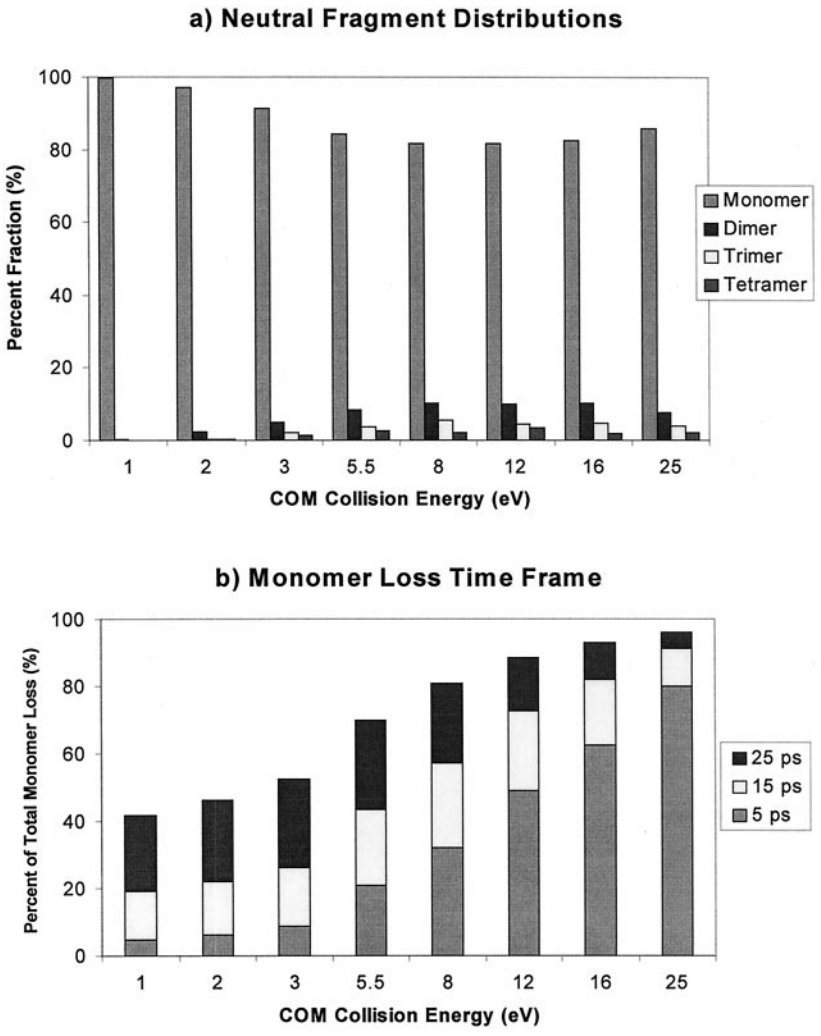

Fig. 2. (a) The observed neutral fragment distribution at each collision energy. Note the minimum in monomer production at 8.0 eV is concurrent with maxima in dimer and trimer production. (b) A bar graph depicts the time frame of monomer loss. At the higher energy collisions, most of the solvent monomers are lost within 25 ps of impact, reflecting the ballistic nature of the collision.

whereas evaporative loss appears to be more important in the low energy regime. These two distinct behaviors suggest the existence of two different collisional processes: a low energy viscid collision and a high energy ballistic collision [24]. Lastly, these results indicate lower evaporation rates than were cited in our earlier analysis [24] and reflect the more stringent evaporation criteria used in the present work.

3.2. Dependence of cluster ion properties on collision energy

Numerous properties of the cluster ions were calculated for each simulation, including the translational, vibrational, and rotational kinetic energies for the final cluster ion size. Each property was then averaged over all the simulations conducted at a specific collision energy that resulted in the same final

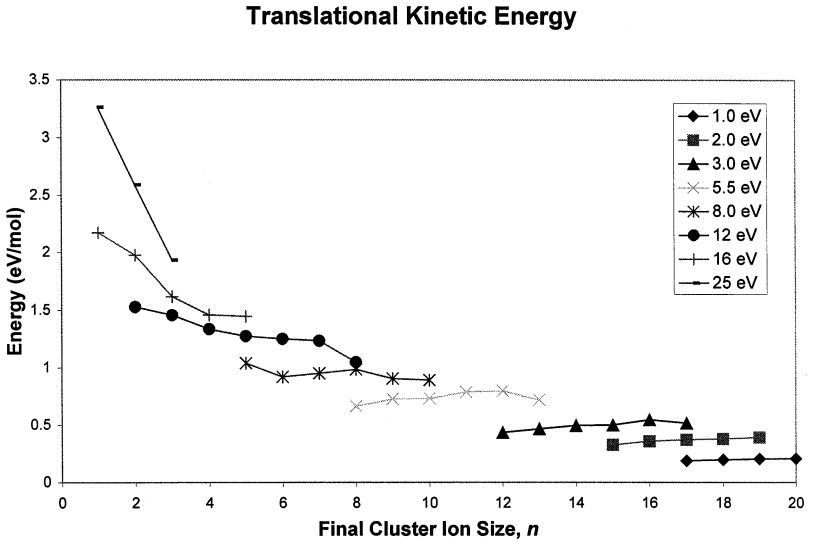

Fig. 3. The average translational kinetic energy at the different collision energies. At lower collision energies, the translational energy remains almost constant regardless of final cluster ion size in accord with experimental observations.

ion cluster size. For example, at a collision energy of 8 eV, 69 out of the 500 simulations resulted in a final ion cluster size of 7. The calculated cluster ion properties were averaged over all 69 simulations to determine the mean value of the desired quantity.

A plot of the variations in cluster ion translational kinetic energy with collision energy is given in Fig. 3. Overall, increasing the collision energy yields a corresponding increase in cluster ion translational energy. However, the collisions at lower energy ($\leq$ 8.0 eV) suggest a uniform translational energy for all of the cluster ions formed at a given energy. This somewhat surprising result has been confirmed experimentally by studies on $Na^+(CH_3OH)_n$ in our laboratory that show a uniform translational energy for all sizes n = 2–16 [38]. At higher collision energies ($\geq$ 12 eV), the translational energy of the cluster ions increases with decreasing size. These trends in the translational energy are indicative of the two distinct collisional processes mentioned earlier.

In the low energy viscid collisions, the neutral cluster envelops the ion upon approach. Nearly all of the methanol molecules initially remain with the ion and consequently the translational velocity of the nascent cluster ion is determined at this point by conservation of momentum. Any evaporative loss of solvent molecules occurs isotropically and thus does not significantly affect the average velocity of the cluster ions with the resultant translational energy of the ion cluster ensemble remaining constant [38]. The ion cluster distribution will evolve and stabilize through evaporative loss at this nearly constant velocity over the 100 ps simulation. The higher energy collisions reflect a ballistic impact by the ion, in effect, shattering the neutral cluster into fragments. As the ion passes through the cluster transferring a significant portion of its kinetic energy, a few solvent molecules may adhere to the ion. As more molecules remain with the ion, the resultant translational velocity of the cluster ion is reduced, directly leading to the observed decrease in translational energy with increasing cluster size. Thus for both regimes, the first few picoseconds of the collision, in which the initial number of methanols solvating the ion is established, determine the ultimate velocity of the cluster ion. The two distinct collisional processes are depicted in the series of pictures in Fig. 4 where several snapshots of collisions occurring at 2.0 and 16.0 eV are contrasted.

A second property of interest is the vibrational kinetic energy content of the cluster ion. Overall, a

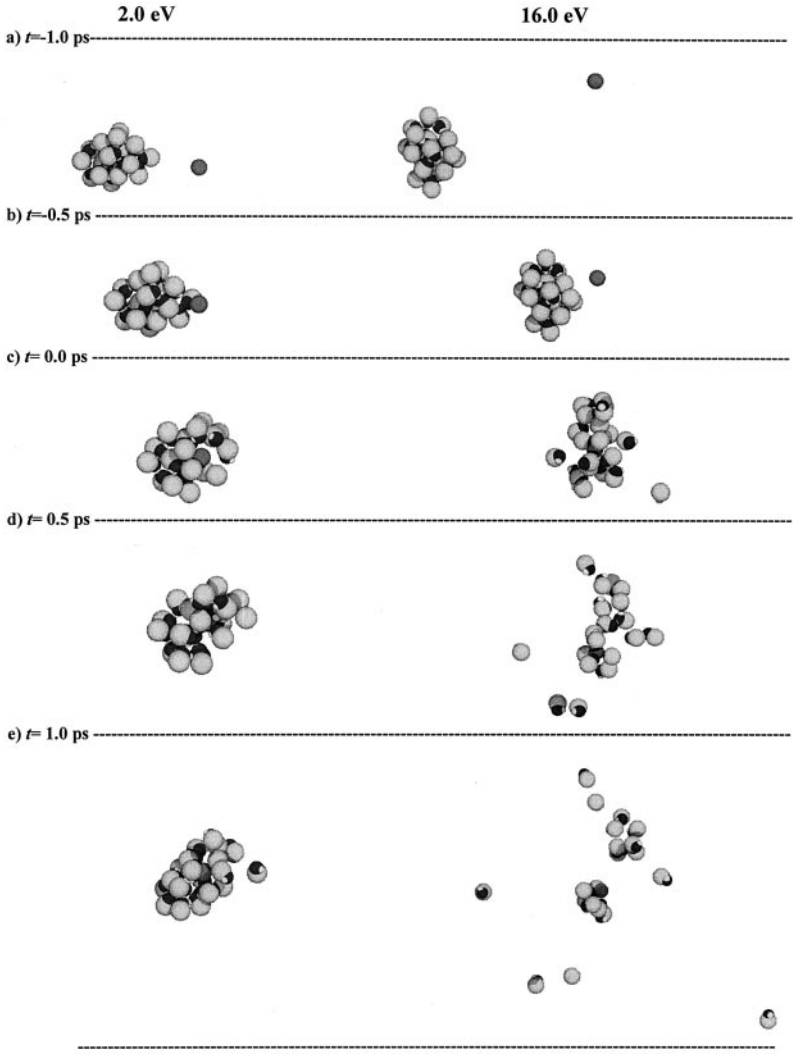

Fig. 4. Series of pictures depicting the collision of a Cs^+ ion with a $(CH_3OH)_{20}$ cluster at collision energies of 2.0 (left-hand side) and 16.0 eV (right-hand side). The position of the ion in each frame is vertically aligned with the ion position in the first frame. The viscid vs. ballistic nature of the impacts is readily observed.

trend toward higher vibrational kinetic energy with increasing cluster size is observed, as shown in Fig. 5(a). The larger cluster ions contain more vibrational energy because of the increase in vibrational degrees of freedom. Aside from this monotonic increase in vibrational energy, the cluster ions also show a dependence on the initial collision energy for a given cluster size, n. This is most clearly visible in the low energy regime, where lower initial collision energy results in lower vibrational kinetic energy content of the cluster ion. An example is the $n = 17$ cluster ion, where the vibrational energy varies from a low of 1.51 eV mol^{-1} at 1 eV collision energy to 1.91 eV mol^{-1} at 3 eV collision energy, a difference of 26%. In the high energy regime, at $n = 2$, the observed increase is 21% between the 12 eV collision at 0.29 eV mol^{-1} and the 25 eV collision at 0.35 eV mol^{-1}. This is an obvious reflection of the amount of kinetic energy available to the system. At this point, it is useful to consider the approximate vibrational temperature of

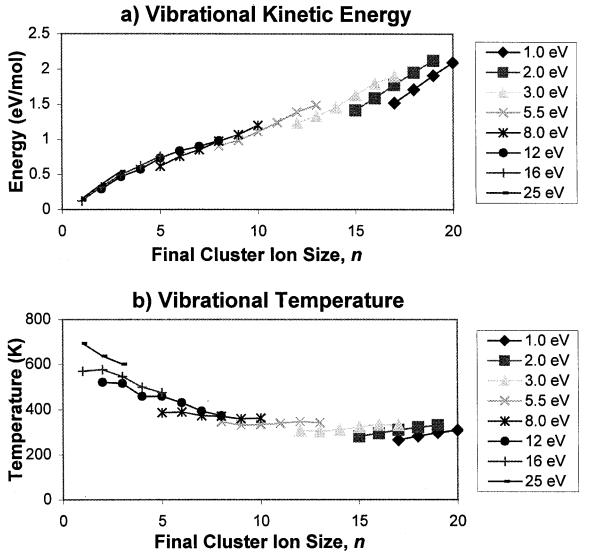

Fig. 5. The size and collision energy dependence of (a) the kinetic vibrational energy, and (b) the vibrational temperature of the final cluster ions. Although the total vibrational energy of the cluster ion decreases with increasing collision energy, the average vibrational energy per mode increases as indicated by the vibrational temperature plot.

the cluster ions, based on Eq. (14). This will allow a more direct comparison between different cluster sizes, as shown in Fig. 5(b). The low energy, viscid collisions ($\leq$ 8.0 eV) yield cluster vibrational temperatures that extend over a range of $\sim$ 300–400 K whereas the higher ballistic collision energies ($\geq$ 12.0 eV) yield vibrational temperatures over a much larger range of 400–700 K. A second difference is also observed in that a small increase in vibrational temperature is observed with increasing cluster size for viscid collisions, whereas the opposite trend is seen in the higher energy collisions. In the former process, the final ion clusters lose methanol monomers to evaporative loss. The evaporated fragment necessarily removes kinetic energy from the system, leaving less energy to be partitioned among the different degrees of freedom. This is a direct observation of evaporative cooling of the cluster ions. At the other extreme, the kinetic energy that remains with the cluster ions is partitioned among the vibrational modes. The more solvents that remain adhered to the ion after collision, the more vibrational modes available, resulting in less energy per mode and a decreased vibrational temperature. The situation is magnified for the smaller ions by a sharp increase in the relative number of vibrational modes that scale as $8n - 3$ where n is the number of methanols solvating the ion.

Rotational motion of the cluster constitutes the third and smallest reservoir of kinetic energy for the ion. Presented in Fig. 6, the rotational kinetic energy displays a trend of decreasing energy with increasing cluster size. Statistical and dynamical processes contribute to the observed trend. Since the number of rotational degrees of freedom remains constant, they represent an ever-decreasing percentage of the total degrees of freedom as the cluster size increases. Dynamically, as will be expounded upon later, fragmentation and dissociation of the cluster ion increases the rotational kinetic energy of the corresponding cluster ion. Thus, the higher collision energy simulations, which yield smaller clusters that undergo more dissociation, will exhibit higher rotational kinetic energies. A plot of the rotational temperature (not shown) displays the same trend. The rotational temperatures encompass a range of 1000–25 K from the smallest to the largest size cluster ion, respectively.

It is important to note that both the vibrational and rotational kinetic energy content as well as the translational energy content of the cluster ions are effected by approximations made in the modeling of the collisions. By using a united atom model for the methyl group, we have removed the methyl group C–H stretches, the methyl group torsional mode, and five other related vibrational modes. This ultimately leads to a smaller available bath for the distribution of energy in the cluster ion and effectively exaggerates the amount of energy found in the cluster ion translational energy, decreasing the amount in the vibrational modes. The zero impact parameter approximation also affects the amount of angular momentum in the cluster ion and will be further discussed below.

An interesting observation is made when plotting the total kinetic energy of each cluster ion at the various collision energies [Fig. 7(a)]. Except for the highest collision energy, all the simulations yield final cluster ions with a total kinetic energy content between 1.5–2.5 eV mol^{-1}. Although the distribution of

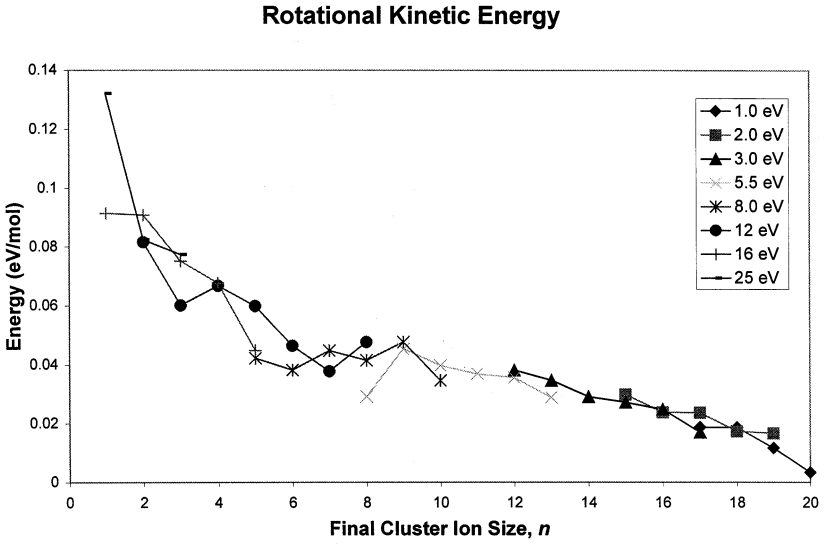

Fig. 6. Average rotational kinetic energy variation with collision energy and cluster ion size.

the kinetic energy among the translational, vibrational, and rotational modes is different at each energy, their sum falls over a fairly narrow range. In addition, with the exception of the two highest collision energies, each collision energy exhibits a trend to lower total kinetic energy with smaller final ion cluster size.

To better understand the distribution of kinetic energy following the collision, the kinetic energy of the entire system (the energy of all the fragment methanol molecules and the cluster ion) was calculated. The fraction of the total system kinetic energy contained in the final ion cluster is plotted in Fig. 7(b) as a function of cluster size and collision energy. The differences between the viscid and ballistic collisional processes are clear. Not surprisingly, the low energy collisions retain most of the total kinetic energy of the system. This is simply because the cluster ion comprises most of the system due to little fragmentation at the lower collision energies. However, the trend lines for the lower collision energies have a large positive slope indicating that the cluster ions formed at low energy contain a greater percentage of the total system kinetic energy as the cluster size increases. This reflects a more statistical distribution of the energy in the viscid collisions. Upon impact, the ion is solvated and few methanol molecules are lost. The cluster slowly stabilizes and evolves through statistical unimolecular loss of solvent molecules, i.e. the clusters evaporatively cool. This allows the excess energy to redistribute among all the available degrees of free-

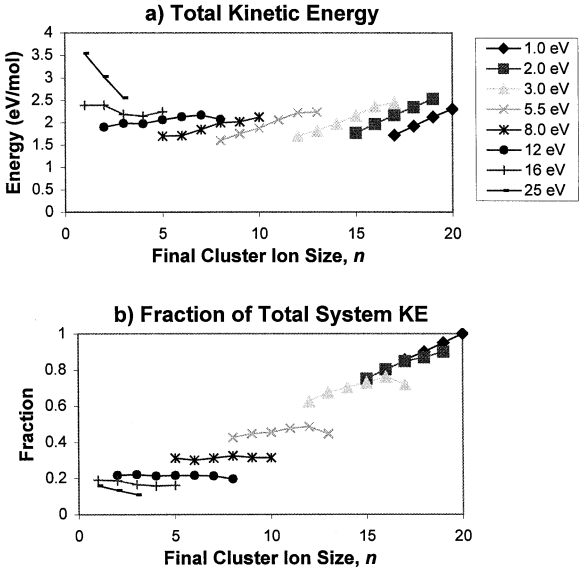

Fig. 7. Cluster ion kinetic energy dependence (a) as a function of size and collision energy and (b) as a fraction of the total available kinetic energy.

dom. As each molecule evaporates, it retains a certain percentage of the available energy, lowering the kinetic energy left in the final cluster ion. This statistical redistribution of the excess kinetic energy is not available in the ballistic collisional process where the dynamics of the ion collision dictate the cluster properties. In the high energy collisions, the cluster ions retain a constant amount of the total available energy regardless of the final size.

3.3. Cluster ion ensemble evolution at a collision energy of 8 eV

The time evolution of the cluster ion ensembles at a single collision energy involves the parent and grandparent ensembles, previously defined, that lead to the final cluster ion distribution. The collisional process is displayed below, schematically, with asterisks denoting each species of specific interest. The sample time of the final ion cluster was defined as the time between the last observed evaporative event and the end of the simulation, as described earlier. The survival time of the corresponding parent and grandparent cluster ions are similarly defined by their respective evaporative events. Since the calculated evaporation times are only accurate to within ~ 0.5 ps, any sample or survival times smaller than 1 ps were not included in the overall statistical calculation for the cluster

$$\begin{aligned} &\overset{\text{Initial Impact}}{Cs^+ \Rightarrow (CH_3OH)_{20}} \rightarrow \cdots \rightarrow {}^*Cs^+(CH_3OH)_{n+2} + CH_3OH \rightarrow \\ &{}^*Cs^+(CH_3OH)_{n+1} + {}^*CH_3OH \rightarrow {}^*Cs^+(CH_3OH)_n + {}^*CH_3OH \end{aligned} \quad (17)$$

Third to Last Evaporation; Penultimate Evaporation; Final Evaporation

The energetics of finite-sized systems can be readily developed using the evaporative ensemble approach formulated by Klots [13–15], where each cluster ion is required to undergo at least one evaporative loss. By using the parent ion, $n + 1$, distributions, we not only ensure that the system is representative of the evaporative ensemble, but also establish a specific time window to serve as the basis of evaluation for the dynamical features of interest. Parent ion cluster lifetimes are determined by fitting the decay of the parent ion population to an exponential decay. A sample fit is presented in Fig. 8(a) for the 1.0 eV collision energy simulations yielding a final ion cluster of size 19. The resulting parent cluster lifetimes over all collision energies are shown in Fig. 8(b). The times are remarkably uniform considering the range of collision energies and size of the cluster ion, with a slight trend to longer lifetimes at lower collision energies. This is to be expected for the evaporative ensemble of cluster ions included in the penultimate evaporation period. The lifetime of the cluster ion is inversely related to the cluster ion vibrational temperature. Since cluster ions formed by the lower energy collisions are vibrationally cooler (Fig. 5), they have slightly longer lifetimes.

Previously, the properties of the final ion cluster were analyzed with respect to their dependence on the COM collision energy. We now look to see how those same properties progress over the course of the 100 ps simulation as the grandparent ensemble evolves into the parent ensemble, which in turn evolves into the final cluster ion ensemble. For simplicity, we need to choose a single collision energy to examine in detail. Based on laboratory experimental conditions that suggest a lab frame collision energy of ~ 10–15 eV, we chose the 8 eV COM collision simulations (Table 3). The 8 eV simulations also provide the largest distribution of final ion cluster sizes for analysis.

The total kinetic energy of the three cluster ion ensembles is displayed in Fig. 9(a). The final cluster ion size is used to enumerate the parent and grandparent ion clusters, thus the $n = 5$ final cluster, the $n = 6$ parent cluster, and the $n = 7$ grandparent cluster are all plotted along the $n = 5$ ordinate. As expected, the grandparent cluster ions contain the most kinetic energy followed by the parents and the

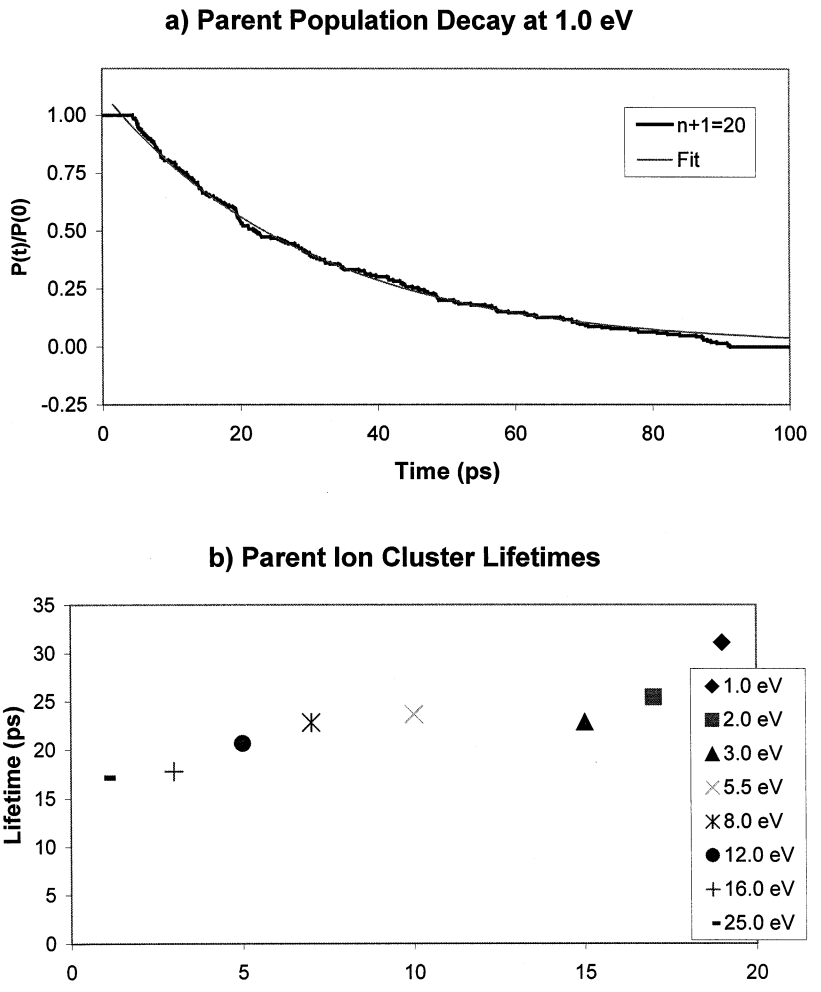

Fig. 8. (a) The decay of the parent ion population with the associated nonlinear least squares fit to a first order exponential decay. The plot depicts the decay of the parent ion, $Cs^+(CH_3OH)_{20}$ to $Cs^+(CH_3OH)_{19}$ at 1.0 eV collision energy. The exponential decay time is 29.6 (0.1) ps. (b) Collision energy and size dependence of parent cluster ion lifetimes displaying a slight increase with cluster ion size. The abscissa denotes the final cluster size; the actual parent cluster ion size is one greater.

final cluster ions. On average, each evaporative event removes $\sim$ 0.20 eV mol^{-1} from the total kinetic energy of the cluster ion. Unfortunately, there are no experimentally measured binding energies for $Cs^+(CH_3OH)_n$ clusters, however, based on the bulk enthalpy of vaporization, a value of $\sim$ 0.4 eV mol^{-1} can be estimated for the larger ($n > 5$) clusters. For the smaller clusters, the binding energy will be higher and range up to $\sim$ 0.6 eV for $Cs^+(CH_3OH)_1$ based on the binding energies available for $Cs^+(H_2O)_n$ clusters [39]. As seen in Fig. 9(a), the final cluster ions contain between 1.7 and 2.1 eV mol^{-1} of energy, sufficient energy to support the further evaporative loss of solvent molecules.

Plots of the variation in translational and vibrational kinetic energy (not shown) exhibit trends similar to the total kinetic energy, with the grandparent clusters ions containing the largest amount of kinetic energy, and the final cluster ions the least. Surprisingly, the situation reverses for the rotational kinetic energy as shown in Fig. 9(b), where each evaporative event leads to a larger rotational kinetic energy for the

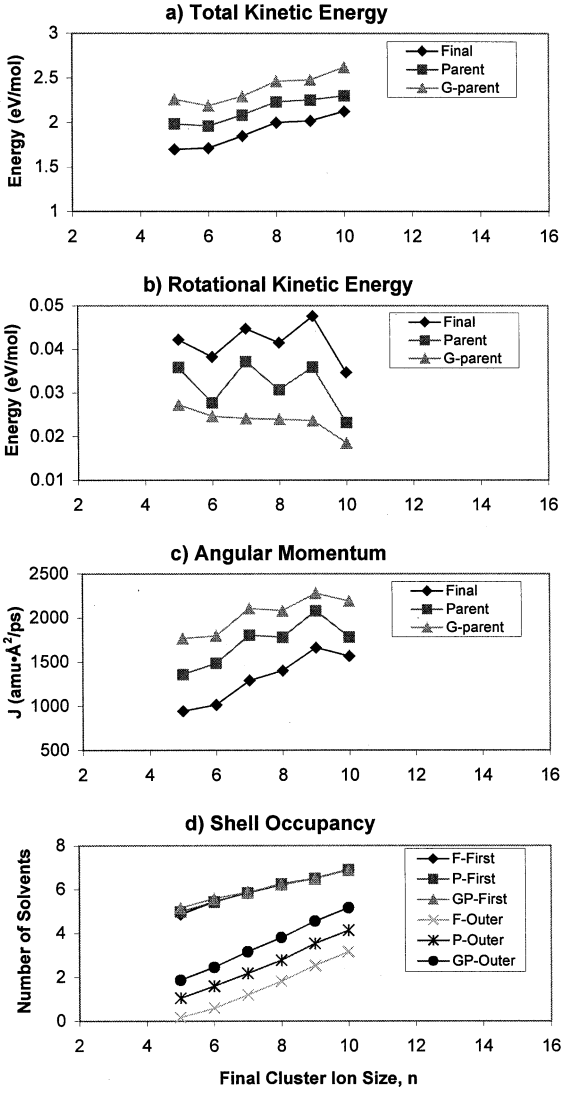

Fig. 9. Evolution of several system properties following evaporation. (a) The total kinetic energy of the cluster ion decreases with each evaporative event. (b) The rotational kinetic energy displays the opposite behavior, unexpectedly increasing with each evaporative loss. (c) Since the angular momentum of the cluster decreases with each evaporative loss, the increase in rotational kinetic energy in (b) must arise from a significant decrease in the cluster moment of inertia [see Eq. (8)]. (d) Each evaporative loss decreases the occupancy of the outer solvation shells, which is responsible for the substantial decrease in the cluster moment of inertia.

product ion. Since the rotational kinetic energy is calculated as $\mathbf{J}^2/2\mathbf{I}$, the evaporative loss must either lead to an increase in the angular momentum of the cluster or a decrease in the cluster moment of inertia. As shown in Fig. 9(c), the angular momentum decreases with each evaporative loss. Thus, the increase in rotational kinetic energy must arise from a substantial decrease in the cluster ion moment of inertia that must be attributed to the loss of a solvent molecule from the outer solvation shells around the ion. This is corroborated by integration of the calculated radial distributions yielding the number of solvents occupying the first and outer solvation shells. The results are charted in Fig. 9(d). The data indicate that the evaporative evolution of the cluster ion ensembles does not affect the first solvent shell configuration. The outer shell occupancy, however, is significantly reduced. Each evaporative event leads to the loss of an outer shell solvent, in turn reducing the moment of inertia of the cluster ion and thus explaining the increase in rotational kinetic energy observed earlier. This confirms that the first shell solvent molecules are more securely bound to the ion core than the outer shell solvents.

When we examine the energy content per degree of freedom in Fig. 10, we find that although the vibrational temperature decreases as one would expect and is theorized by the evaporative ensemble, the rotational temperature *increases* upon evaporation. This interesting result sheds some light on a couple of key issues. First, collisions at zero impact parameter can only generate cluster ions with angular momentum if the neutral fragments carry off an equal and opposite amount of angular momentum since the initial neutral $(CH_3OH)_{20}$ cluster begins rotationally cold. After the initial collision and the subsequent loss of neutral fragments, the cluster ion is indeed imparted some angular momentum as confirmed by Fig. 9(c). [Note the exception will be the $Cs^+(CH_3OH)_{20}$ cluster ions at 1.0 eV collision energy where no solvent loss is experienced. This cluster ion contains rotational energy equivalent to a temperature of $\sim$ 26 K, from Fig. 6 and Eq. (13), that comes from the initial 25 K equilibration of the neutral cluster.] As the nascent cluster ion evolves and undergoes evaporative cooling, the various vibrational and rotational degrees of freedom are expected to equilibrate. This necessitates a decrease in the vibrational energy and a concurrent

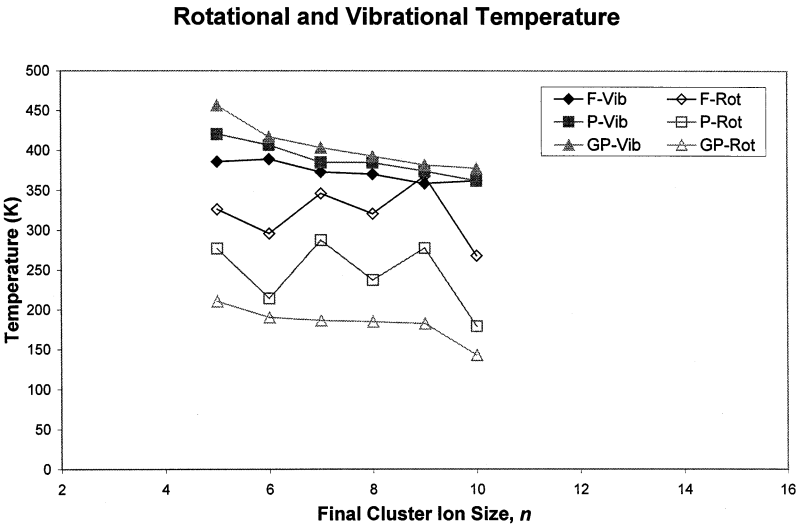

Fig. 10. The convergence of rotational and vibrational temperatures observed during successive evaporative events at a COM collision energy of 8.0 eV.

increase in the rotational energy. As can be seen from Fig. 10, the rotational and vibrational temperatures are converging with each successive evaporation. The evaporative loss of a solvent molecule is the mechanism by which the rotational and vibrational temperature distributions converge. This is a fitting confirmation of the evaporative ensemble in that the exact nature of the initial distribution is lost after a number of evaporative events. A longer observation time scale would of course be needed to determine the extent of thermal equilibration between the vibrational and rotational degrees of freedom. Last, as seen in Fig. 9(d), evaporation occurs from the outer solvent shell, where the molecules are most weakly bound. The population of bending vibrational modes in the transition state will lead to a change in the angular momentum of the product cluster ion, so equilibration between the physically coupled rotational and vibrational degrees of freedom is expected.

3.4. Time scale of ion solvation

The third and final aspect of the collision simulations is the time scale of ion solvation. The time required for collisional solvation can be inferred from the time-dependent radial distribution functions (RDFs). Because the size of the first solvation shell for the $Cs^+(CH_3OH)_n$ system is $\sim$ 10 [22] on the microsecond time scale of our experiments, we focused attention on the time needed to establish a first solvent shell about the Cs^+. The formation of a solvation shell is defined by a distinct maximum in the Cs^+-oxygen RDF. This is valid for collision energies of 8 eV or less, where the ion clusters have a sufficient number of methanols to form a nearly completed shell. Plots of the time dependent RDFs are displayed in Fig. 11. At a collision energy of 2.0 eV [Fig. 11(a)], the resultant average ion cluster contains 17 methanols. This is sufficient to ensure the filling of the first solvent shell about the ion and mark the radial boundaries of the first solvent shell. Within 1 ps of collision, a definitive structure is observed in the RDF. The first peak in the RDF occurs at 2.7 Å and corresponds to methanols in the first solvent shell around the ion. A second broader peak is centered about 6.0 Å and is attributed to methanols in a second solvation sphere outside the first shell. By $t = 3$ ps, the peak corresponding to the first shell becomes better defined and the second broader peak resolves into a more distinct peak centered at 5.5 Å due to

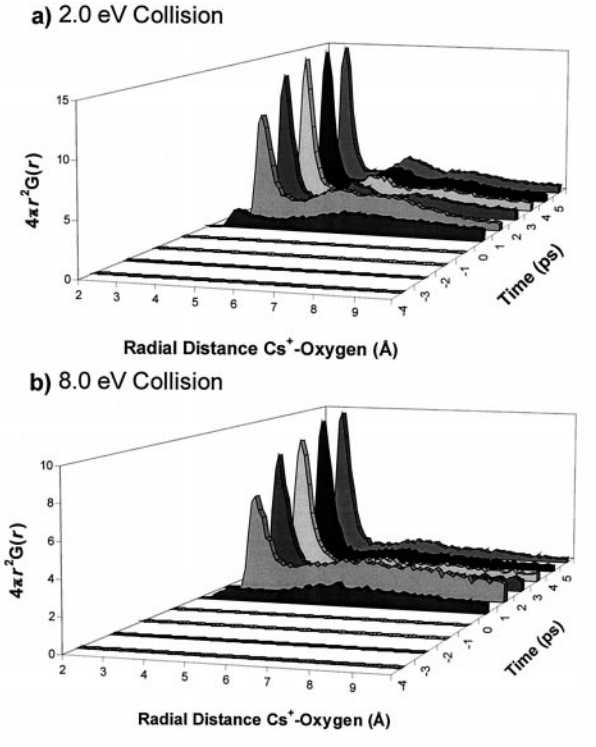

Fig. 11. Radial distribution functions as a function of time at (a) 2.0 eV collision energy and a final cluster ion of size $n = 17$ and at (b) 8.0 eV with a final cluster ion size of $n = 7$. The large sharp peak located near 2.7 Å is attributed to the formation of the first solvent shell. A distinct second solvent shell is also observed at 5.5 Å in part (a). At both energies the solvent shell structure forms within picoseconds of impact.

methanols in a second shell around the ion. The RDFs indicate that the bulk of the first solvation shell forms within 2 ps of the impact. Five ps after the impact, the RDFs remain relatively constant for the remainder of the simulation, with small variations attributed to the evaporative loss of solvent. Rapid solvent shell formation is indicative of the strong interaction between the methanol and the cesium ion. At higher collision energies, the times required for the formation of the solvent shell are slightly longer, as shown in Fig. 11(b) for the collision at 8.0 eV. However, the process is still very rapid.

Calculating the average orientation of the solvent dipole moment vector as a function of time, $\langle \hat{\mu} \cdot \hat{r} \rangle(t)$, serves as a second quantitative measure of the solvation time scale. Prior to impact with the ion, the random orientation of the methanols leads to an average value of zero. Full alignment would return a value of one. As can be seen by Fig. 12, upon collision the ion has an immediate effect on the orientation of the methanols, substantiating the rapid solvent shell formation time indicated by the time dependent RDFs. The first plot, Fig. 12(a), displays the orientation function averaged over all 20 methanol molecules. Within a single picosecond of the impact, a majority of the solvents are oriented towards the ion. As the dissociated or evaporated methanols depart from the ion over time, the value of the orientation function decreases, with an asymptotic limit determined by the number of methanols that remain about the ion. The increase in $\langle \hat{\mu} \cdot \hat{r} \rangle(t)$ with the final number of solvents shows the ability of the ion to influence, either directly or indirectly, the orientation of all of the molecules about the ion. It is also useful to select and observe the behavior of only those molecules that are retained by the ion at the end of the simulation, as shown in Fig. 12(b). The dipole orientation of the smaller ion clusters tends closer towards unity because of the stronger interaction between the methanols and the ion. As the ion is surrounded by more methanols, the degree of orientation is slightly reduced. There are two possible causes for this effect. As the number of solvents increase, the ion is more effectively shielded and the electrostatic interaction is slightly weakened. Additionally, molecules can now occupy the second solvent shell, where the intervening first solvent shell screens the influence of the ion. Another interesting aspect of the data is the nonzero average orientation function observed before the ion impact. This suggests that methanol molecules that are favorably oriented towards the ion before impact have a greater probability of adhering and solvating the ion.

4. Conclusions

Molecular dynamics simulations of a Cs^+ ion colliding with a neutral cluster of 20 methanols at zero impact parameter have been performed at eight different COM collision energies ranging from 1–25 eV.

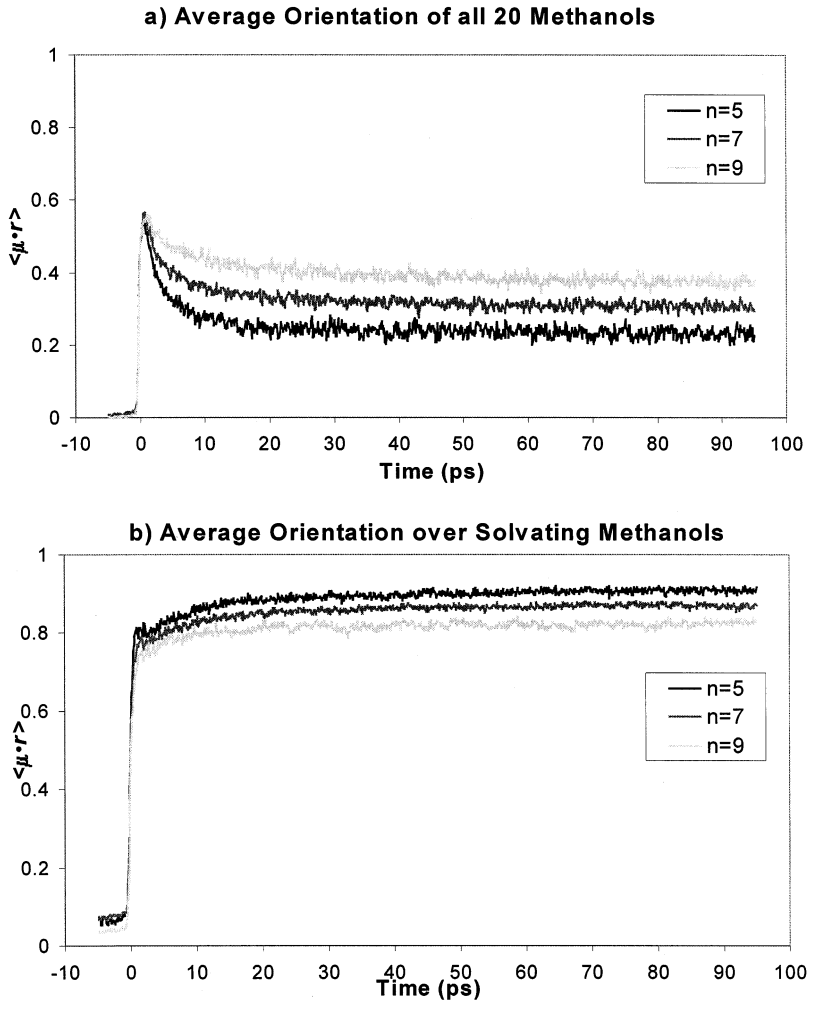

Fig. 12. (a) Average value of the orientation function over all 20 methanol solvents present in the simulation. The value averages to zero before the impact of the ion as expected for a randomly oriented set of solvents. (b) The average value of the orientation function calculated for the methanol molecules that remain solvating the ion at the end of the simulation. Note the nonzero value of the function before impact by the ion, indicating that methanols initially oriented towards the ion will preferentially solvate the ion.

Two collision energy dependent mechanisms of ion cluster formation emerge: at lower collision energies, a viscid collision occurs followed by evaporative methanol loss, whereas at higher energies, the Cs^+ ion achieves a ballistic penetration of the neutral cluster after which only a few solvent molecules remain adhered. The disparate collisional processes have a distinct effect on numerous cluster ion properties including the cluster ion size distribution, the translational, vibrational, and kinetic energy distributions and the partitioning of energy through the cluster ion system. The ion cluster translational energy resulting from a viscid collision is relatively constant, consistent with experimental observations. The higher collision energies lead to vibrationally and rotationally warmer clusters. With the exception of the 25 eV collisions, the total kinetic energy of the cluster ions fall within a range of 1.5–2.5 eV mol^{-1} regardless of the COM collision energy.

The distribution of the neutral fragments at all

collision energies was composed predominantly of methanol monomers. Almost all observed evaporative events led to the loss of methanol monomers. Dimer and larger neutral fragments were primarily formed by the initial ion collision. Reflecting the nature of the fragmentation process, the majority of monomer evaporation occurred rapidly (< 5 ps) at high collisional energies. At low energy, evaporation occurred at a slower pace (> 15 ps).

The evaporative evolution of cluster ions formed at 8.0 eV was also studied. The simulations were divided into different ion cluster windows based on evaporative events. This led to the definition of grandparent, parent, and final cluster ion ensembles. The lifetimes of the parent cluster ions displayed an increase with cluster ion size, reflecting the concomitant decrease in vibrational energy. The cluster translational and vibrational kinetic energy distributions followed the expected trend, with the grandparent ion clusters containing the most kinetic energy, and after two evaporative events, the final cluster ions contained the least. Unexpectedly, the rotational kinetic energy was found to increase with each evaporative event. This was caused by significant decreases in the cluster ion moment of inertia upon the loss of solvent molecules from the outer solvation shells surrounding the Cs^+ ion. This resulted in an increase in rotational temperatures that tended to converge to the vibrational temperatures on the 100 ps time scale of the simulation.

Ion solvation was found to occur within 2 ps of impact, regardless of solvation mechanism or final ion cluster size as determined by time-dependent radial distribution functions. This was corroborated by following the average orientation of the methanol molecule dipole moments over time. Methanols that have their dipoles initially oriented toward the ion prior to collision were found to have a higher probability of adhering to and solvating the ion.

As noted earlier, a number of restrictions made on these simulations: zero impact parameter, single neutral cluster target size, 3-site pairwise additive potential, and 100 ps simulation period, were made for a variety of reasons. These restraints have allowed us to focus on the most basic aspects of ion solvation. As the results have shown, the equilibration of rotation and vibration appears to take place on a time scale of tens of picoseconds. Additional studies to examine the role of impact parameter, target neutral cluster size, and simulation time frame are currently underway. When combined, these studies will provide a clearer picture of cluster ion formation in the gas phase.

Acknowledgements

The authors would like to thank Dr. Corey Weinheimer for the measurement of translational energies of a number of ion cluster systems. The National Science Foundation (CHE-9700722) is gratefully acknowledged for partial support of this research. One of the authors (JML) would also like to extend his thanks to Prof. Mike Bowers for his contributions to the field and for many stimulating discussions shared over the years. The helpful comments and suggestions of the reviewers were greatly appreciated.

References

[1] J.A. Syage, J. Phys. Chem. 99 (1995) 5772.
[2] R.C. Dunbar, J. Phys. Chem. 98 (1994) 8705.
[3] R.C. Dunbar et al., J. Am. Chem. Soc. 117 (1995) 12 819.
[4] R.C. Dunbar, T.B. McMahon, Science 279 (1998) 194.
[5] A. Ferhati, T.B. McMahon, G. Ohanessian, J. Am. Chem. Soc. 118 (1996) 5997.
[6] T. Schindler et al., J. Phys. Chem. 98 (1994) 4316.
[7] T. Schindler, C. Berg, G. Niednerschatteburg, V.E. Bondybey, Chem. Phys. Lett. 250 (1996) 301.
[8] J.A. Draves, J.M. Lisy, J. Am. Chem. Soc. 112 (1990) 9006.
[9] X. Zhang, A.W. Castleman Jr., J. Am. Chem. Soc. 114 (1992) 8607.
[10] T.J. Selegue, J.M. Lisy, J. Am. Chem. Soc. 116 (1994) 4874.
[11] M. Sanekata, F. Misaizu, K. Fuke, S. Iwata, K. Hashimoto, J. Am. Chem. Soc. 117 (1995) 747.
[12] H. Watanabe, S. Iwata, K. Hashimoto, F. Misaizu, K. Fuke, J. Am. Chem. Soc. 117 (1995) 755.
[13] C.E. Klots, J. Chem. Phys. 83 (1985) 5854.
[14] C.E. Klots, Z. Phys. D 5 (1987) 83.
[15] C.E. Klots, J. Phys. Chem. 92 (1988) 5864.
[16] C. Bréchignac, H. Busch, P. Cahuzac, J. Leygnier, J. Chem. Phys. 101 (1994) 6992.
[17] C. Bréchignac, P. Cahuzac, M. de Frutos, O. Garnier, N. Kebaili, J. Chem. Phys. 103 (1995) 6631.
[18] F. Misaizu, M. Sanekata, K. Fuke, S. Iwata, J. Chem. Phys. 100 (1994) 1161.

[19] T.J. Selegue, N. Moe, J.M. Lisy, Z. Phys. D 26 (1993) 207.
[20] T.J. Selegue, J.M. Lisy, J. Phys. Chem. 96 (1992) 4143.
[21] T.J. Selegue, N. Moe, J.A. Draves, J.M. Lisy, J. Chem. Phys. 96 (1992) 7268.
[22] J.A. Draves, Z. Luthey-Schulten, W.-L. Liu, J.M. Lisy, J. Chem. Phys. 93 (1990) 4589.
[23] T.J. Selegue, O.M. Cabarcos, J.M. Lisy, J. Chem. Phys. 100 (1994) 4790.
[24] O.M. Cabarcos, J.M. Lisy, Chem. Phys. Lett. 257 (1996) 265.
[25] F.H. Stillinger, T.A. Weber, Chem. Phys. Lett. 79 (1981) 259.
[26] T.A. Weber, F.H. Stillinger, Chem. Phys. Lett. 89 (1982) 154.
[27] G. Del Mistro, A.J. Stace, Chem. Phys. Lett. 196 (1992) 67.
[28] M. Svanberg, L. Ming, N. Markovic, J.B.C. Pettersson, J. Chem. Phys. 108 (1998) 5888.
[29] B.R. Brooks et al., J. Comput. Chem. 4 (1983) 187.
[30] W.L. Jorgensen, D.L. Severance, J. Chem. Phys. 99 (1993) 4233.
[31] W.L. Jorgensen, J.M. Briggs, M.L. Contreras, J. Phys. Chem. 94 (1990) 1683.
[32] J. Aqvist, J. Phys. Chem. 94 (1990) 8021.
[33] L. Verlet, Phys. Rev. 159 (1967) 98.
[34] M.P. Allen, D.J. Tildesley, Computer Simulation of Liquids, Oxford University Press, Oxford, 1987.
[35] J.-P. Ryckaert, G. Ciccotti, H.J.C. Berendsen, J. Comput. Phys. 23 (1977) 327.
[36] S. Weerasinghe, F.G. Amar, J. Chem. Phys. 98 (1993) 4967.
[37] Y. Lin, C.D. Jonah, Chem. Phys. Lett. 233 (1995) 138.
[38] C.J. Weinheimer, Ph. D. Thesis, University of Illinois, 1998.
[39] R.G. Keesee, A.W. Castleman Jr., J. Phys. Chem. Ref. Data 15 (1986) 1011.